A numerical study of projectile impact on thin aluminium plates

3 authors:

Raguraman Munusamy
Indian Institute of Information Technology, Design & Manufacturing, Kancheepur…
20 PUBLICATIONS   168 CITATIONS

SEE PROFILE

Anindya Deb
Indian Institute of Science
141 PUBLICATIONS   905 CITATIONS

SEE PROFILE

Jagadeesh Gopalan
Indian Institute of Science
297 PUBLICATIONS   2,376 CITATIONS

SEE PROFILE

Some of the authors of this publication are also working on these related projects:

Hypersonic Aerodynamics View project

Effect of shock wave deformation on materials View project

A numerical study of projectile impact on thin aluminium plates

M Raguraman, A Deb and G Jagadeesh

The online version of this article can be found at:

http://pic.sagepub.com/content/223/11/2519

Published by:

$SAGE

http://www.sagepublications.com

On behalf of:

Institution of MECHANICAL ENGINEERS

Institution of Mechanical Engineers

Additional services and information for *Proceedings of the Institution of Mechanical Engineers, Part C: Journal of Mechanical Engineering Science* **can be found at:**

Email Alerts: http://pic.sagepub.com/cgi/alerts

Subscriptions: http://pic.sagepub.com/subscriptions

Reprints: http://www.sagepub.com/journalsReprints.nav

Permissions: http://www.sagepub.com/journalsPermissions.nav

Citations: http://pic.sagepub.com/content/223/11/2519.refs.html

>> Version of Record - Nov 1, 2009

What is This?

A numerical study of projectile impact on thin aluminium plates

M Raguraman[1]*, **A Deb**[2], and **G Jagadeesh**[3]

[1]School of Mechanical Engineering, University of Leeds, Leeds, UK

[2]Centre for Product Design and Manufacturing, Indian Institute of Science, Bangalore, India

[3]Department of Aerospace Engineering, Indian Institute of Science, Bangalore, India

Abstract: This article deals with a simulation-based study of the impact of projectiles on thin aluminium plates using LS-DYNA by modelling plates with shell elements and projectiles with solid elements. In order to establish the required modelling criterion in terms of element size for aluminium plates, a convergence study of residual velocity has been carried out by varying mesh density in the impact zone. Using the preferred material and meshing criteria arrived at here, extremely good prediction of test residual velocities and ballistic limits given by Gupta *et al.* (2001) for thin aluminium plates has been obtained. The simulation-based pattern of failure with localized bulging and jagged edge of perforation is similar to the perforation with petalling seen in tests. A number of simulation-based parametric studies have been carried out and results consistent with published test data have been obtained. Despite the robust correlation achieved against published experimental results, it would be prudent to conduct one's own experiments, for a final correlation via the present modelling procedure and analysis with the explicit LS-DYNA 970 solver. Hence, a sophisticated ballistic impact testing facility and a high-speed camera have been used to conduct additional tests on grade 1100 aluminium plates of 1 mm thickness with projectiles of four different nose shapes. Finally, using the developed numerical simulation procedure, an excellent correlation of residual velocity and failure modes with the corresponding test results has been obtained.

Keywords: residual velocity, ballistic limit, projectile, aluminium plate, numerical simulation

1 INTRODUCTION

The behaviours of armour plates under projectile impact have been studied experimentally [1–7], using analytical/semi-empirical formulations [2, 6], and numerically [8–15]. Among these three approaches, the numerical analysis procedure consisting of non-linear finite element-based analysis appears to be the most versatile tool for predicting ballistic limits of projectiles for impact on armour plates.

The normal and oblique impacts on single and layered mild steel plates with jacketed hard-core projectiles have been studied experimentally by Gupta and Madhu [1]. Gupta *et al.* [2] have studied normal impact on thin aluminium plates by ogival-nosed projectiles at impact velocities greater than the ballistic limit. For a plate of a given material, these investigators [1, 2] have studied the effects of plate thickness and projectile-related parameters on residual velocity and ballistic limit. Oblique impact of the projectile on thin aluminium plates has been investigated experimentally by Khan *et al.* [3]. Based on the experimental results, Khan *et al.* [3] have developed an analytical model for predicting the residual velocity and ballistic limit. Gupta *et al.* [4] have studied the behaviour of thin aluminium plates subjected to impact by blunt- and hemispherical-nosed projectiles for velocities in the range of $\sim$60–120 m/s using both experimental and numerical approaches. Corran *et al.* [5] have studied experimentally the impact of

**Corresponding author: School of Mechanical Engineering, University of Leeds, Woodhouse Lane, Leeds, West Yorkshire LS2 9JT, UK. email: r.munusamy@leeds.ac.uk*

projectiles at sub-ordnance velocities against mild steel, stainless–steel, and aluminium plates. The projectile mass as well as nose shape and plate thickness were found to have an important effect on penetration. Backman and Goldsmith [**6**] have presented a detailed survey of the mechanics of penetration of projectiles into targets. They have provided insight into perforation mechanisms of plates subject to ballistic impact with schematics and experiment-based snapshots. Borvik *et al.* [**7**] have carried out experiments on perforation of 12 mm thick steel plates by 20 mm diameter projectiles with different nose-shaped projectiles. They found the nose shape of a projectile to significantly affect both energy absorption and failure modes.

It is observed that although experimental studies [**1**–**7**] provide valuable information on performance of plates and projectiles and their mechanics, these can be prohibitively expensive and time-consuming for carrying out parametric studies with a number of variables involved and, consequently, for obtaining an optimized design.

Many researchers have reported simulation-based prediction of residual velocities for the impact of projectiles with velocities greater than ballistic limit on metallic and non-metallic plates. The main objective in these studies was to show that analysis results can correlate against experimental data. A bulk of these simulations employ plane strain or axisymmetric elements [**8**–**16**] with the help of which primarily normal impact on flat targets with velocities higher than ballistic limits can be represented. For simulating impact on thin plates or membrane-type targets, the latter have been sometimes modelled with shell elements. Occasionally, the target plates have also been modelled with three-dimensional elements, which are necessary for representing the behaviours of thick and multi-layered plates. Various materials for plates have been considered for simulation-based studies: Kad *et al.* [**8**] discussed material modelling procedure for textured Ti-6Al-4V plates; Lim *et al.* [**9**] studied numerically the penetration of Twaron fabric; Tan *et al.* [**10**] studied the penetration of Twaron fabric; glass fibre-reinforced plastic (GRP) plates as targets were considered by Nandall *et al.* [**11**]; mild steel and aluminium plates were considered by Park *et al.* [**12**] for illustrating their optimization algorithm; Fawaz *et al.* [**13**] investigated the performance of ceramic-composite armours subjected to normal and oblique impact by projectiles; Borvik *et al.* [**14**] used 460 E steel plates in their studies and incorporated a damage parameter in the modified Johnson–Cook constitutive model; and impact on HSLA-100 steel plates using quasi-static and temperature-independent material properties were considered by Martineau *et al.* [**15**]; Prakash *et al.* [**16**] implemented an algorithm to carry out the adaptive finite-element analysis of plastic deformation of plates during impact of projectiles.

It appears from the references mentioned above that a primary focus in numerical simulations of ballistic impact on plates has been material modelling. However, in finite-element analysis, a number of other factors such as element size, target thickness, impact velocity, and contact algorithm can influence the computed results. Hence, unless the effects of the key factors that control the outcome of analysis are separately evaluated and convergence and accuracy of responses, such as residual velocity, are established, it would be difficult to say that a given finite-element modelling procedure is satisfactory for application to design problems for which no experimental data are available for correlation.

In the present study, plates are represented with shell elements and projectiles with solid elements. Published data on stress–strain behaviours of an aluminium alloy (Al 6061 T6) have been used to generate the strain rate dependence of yield and failure stresses of the target plate material (Al 1100 H14) studied here. This procedure of material modelling with a von Mises-type yield criterion and isotropic strain hardening can be appealing to design engineers for its inherent simplicity. While material modelling is a key consideration in analysing the mechanics of projectile and target interaction, other parameters such as mesh density cannot be ignored. In order to establish the required modelling criterion in terms of element size, a convergence study of residual velocity has been carried out by varying mesh density in the impact zone. Additionally, the effect of using quasi-static properties only of the plate material without considering strain rate sensitivity is shown to yield residual velocities that are significantly higher than the corresponding test velocities. Using the preferred material and meshing criteria arrived at here, extremely good prediction of test residual velocities and ballistic limits given in reference [**2**] for thin aluminium plates has been obtained. The simulation-based pattern of failure with localized bulging and jagged edge of perforation is similar to the perforation with petalling seen in tests. A number of simulation-based parametric studies have been carried out and results consistent with published test data have been obtained. For further validation, experiments on grade 1100 aluminium plates of 1 mm thickness with projectiles of four different nose shapes have been conducted. A sophisticated ballistic impact testing facility and a high-speed camera have been used in the present impact tests. Finally, using the developed numerical simulation procedure, an excellent correlation of residual velocity and failure modes with the corresponding test results has been obtained.

It may be noted that few similarities have been observed when compared with the procedure outlined in references [**17**] and [**18**]. These studies [**17**, **18**] were mainly for simulating the behaviour of moderately thick (4.7–16 mm) square-shaped mild steel plates

subjected to normal impact of ogival-nosed projectiles for the ordnance velocity range of ~800–870 m/s. However, this article describes the new approach for simulating the impact behaviour of projectiles on thin circular aluminium plates of 1 mm thickness for low range velocities of ~20–80 m/s. The impact conditions of the mild steel target plates in references [17] and [18] and the present aluminium plates are very different, including failure patterns that indicated a need for the development of new guidelines. Hence, a new simulation procedure has been developed and the same is presented in this article. It is pointed out that the experiences gained earlier for mild steel plates were fully used for simulating the present problem. Additionally, a new method of predicting the ballistic limits using numerical simulations is reported.

2 FINITE-ELEMENT MODELLING

Finite-element models of a thin aluminium target plate and a hardened steel projectile using Belytschko–Lin–Tsay (BLT) shell and constant solid elements are shown in Figs 1 and 2, respectively. The plate is circular in shape with a diameter of 255 mm and is clamped along the edges. Plates of three different thicknesses (viz. 0.5, 1.5, and 2.0 mm) are considered. The projectiles are generally of diameter 10 or 15 mm, and are ogival-nosed. The length to diameter (l/d) ratio of 10 mm diameter projectiles varied from 1 to 4 while studying the effect of projectile mass on ballistic limit in the parametric studies carried out. Contact_eroding_surface_surface (CESS) interface is defined for capturing the interaction between the target plate and projectile.
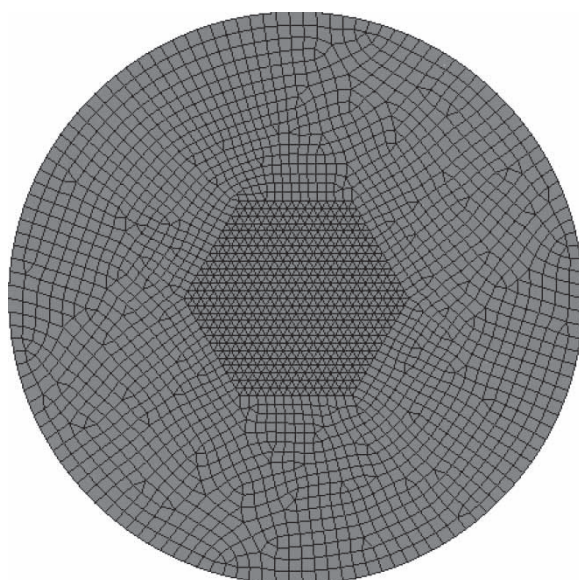
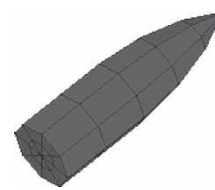

Fig. 1 Plate modelled with shell elements

Fig. 2 Projectile modelled with solid elements

2.1 Material modelling of target plates

Material type 19 in LS-DYNA has been used for defining the behaviour of target aluminium plates studied experimentally in reference [2]. The information furnished in reference [2] on the target plate material indicates that it is closer to Al 1100 H14 alloy (all 1xxx series aluminium alloys are generally known as 'commercial grade' alloys) for which quasi-static properties are given in reference [19]. For further confirmation, a coupon test has been carried out using a commercial 1100 grade alloy test specimen. The geometric details of a standard dogbone specimen for uniaxial test are obtained from reference [20]. Both the ends of the specimen were held firmly between the cross-heads as shown in Fig. 3, and a constant velocity of 20 mm/min, which can generate a strain rate of 0.005 s^{-1}, was applied until fracture occurs. The recorded stress–strain data are shown in Fig. 4 and the properties are compared in Table 1.
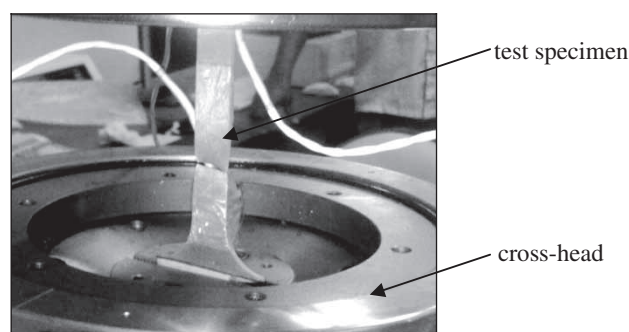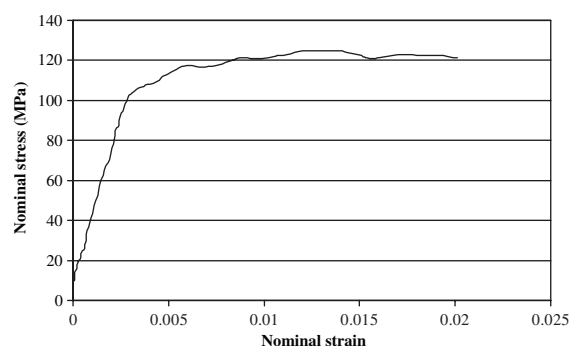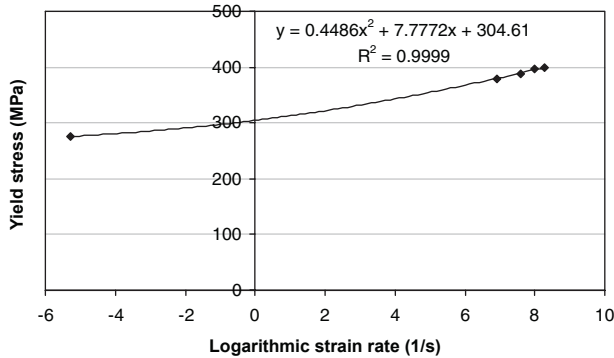

Fig. 3 Test specimen placed between cross-heads

Fig. 4 Recorded nominal properties of commercial 1100 grade alloy

Table 1 Comparison of nominal properties from coupon test and [19]

Properties	From Fig. 3	From ref. [19]
Yield stress (MPa)	116.6	117
Failure stress (MPa)	124.8	124
Failure strain (%)	20	20

The strain-rate-dependent behaviour of these alloys was not readily available. However, test-based values of yield and ultimate strengths at a number of strain rates are mentioned in reference [21] for Al 6061 T6 alloy. The variations of material properties (i.e. yield and ultimate stresses) for this latter alloy can be represented with a fair degree of fidelity to test data with the help of second-order regression polynomials as shown in Fig. 5. These regression polynomials can be used for predicting the yield and ultimate strengths of Al 6061 T6 alloy at any strain rate within the ranges given in Fig. 5. In the equations given in Fig. 5, the value of y represents the true yield or failure stress and x represents the corresponding logarithmic strain rate. The strengths of the plate material (Al 1100 H14 alloy) are then obtained by scaling according to equation (1) in a manner similar to the approach followed earlier for

mild steel plates in references [17] and [18]

$$\sigma_{\dot{\varepsilon}}^{(Al\ 1100\ H14)} = \sigma_{\dot{\varepsilon}_0}^{(Al\ 1100\ H14)} \frac{\sigma_{\dot{\varepsilon}}^{(Al\ 6061\ T6)}}{\sigma_{\dot{\varepsilon}_0}^{(Al\ 6061\ T6)}} \qquad (1)$$

where $\sigma_{\dot{\varepsilon}}$ is the strength (yield or ultimate) at a given strain rate, $\dot{\varepsilon}$ (s^{-1}); and $\sigma_{\dot{\varepsilon}_0}$ is the corresponding quasi-static strength at a low strain rate of $\dot{\varepsilon}_0$ (s^{-1}).

Following the approach outlined above and assuming a constant tangent modulus obtained from the quasi-static true properties of Al 1100 H14 alloy given in Table 2, the bi-linear variations of true stress with respect to true strain are obtained as shown in Fig. 6 and used in material type 19 as mentioned earlier for representing the behaviour of target plate material in finite-element analysis.

It may be pointed out that the true stress and strain at a strain rate of $10\,000\,s^{-1}$ were used in the current simulations and it would be very difficult to measure these stress–strain values at this high strain rate with the available facilities. Hence, a popular extrapolation approach has been adopted to obtain the required stress and strain values. The similar kind of scaling approach was used for mild steel plates earlier in references [17] and [18], which shows the confidence of using the present method of obtaining stress–strain values at different strain rate conditions.

2.2 Material modelling of the projectile

The projectile was modelled with material type 24 in LS-DYNA used for defining piecewise linear

Fig. 5 Regression-based curve fitting of (a) yield stress and (b) ultimate stress of Al 6061 T6 alloy with respect to strain rate

Table 2 Quasi-static nominal and true properties of Al 1100 H14 alloy

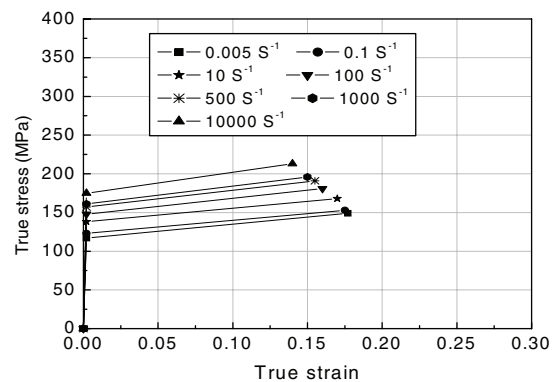| Properties	Nominal value [19]	True value
Yield stress (MPa)	117	117
Failure stress (MPa)	124	149
Failure strain (%)	20	18

Fig. 6 True stress–true strain behaviours at different strain rates of Al 1100 H14 alloy

elasto-plastic behaviour. The hardness of the projectile material specified in reference [2] was found to be comparable to that of AISI A2 tool steel mentioned in reference [19]. Hence the properties of this hardened steel have been chosen for defining the behaviour of projectile in current simulations. The projectile was assumed as rigid by using a very high failure strain in the above material model. Hence, the effect of element size on the projectile modelling is not significant in terms of deformation and the residual velocity predictions. For all analyses carried out here, the visco-plastic formulation option is used for both plate and projectile materials.

3 EFFECT OF ELEMENT SIZE ON PROJECTILE RESIDUAL VELOCITY

The objective of this study is to determine an optimal element size that will yield reliable values of projectile residual velocity. Al 1100 H14 alloy plates of three different thickness have been considered and the computed residual velocities are compared (as shown in Fig. 7) with corresponding test residual velocities reported in reference [2]. It is found that residual velocity tends to converge monotonically in all cases considered, and a nearly circular perforation due to removal of elements in the impact zone is obtained. In order to assess the degree of correlation of simulation-based residual velocities with test residual velocities, the following 'correlation index' (CI) is defined

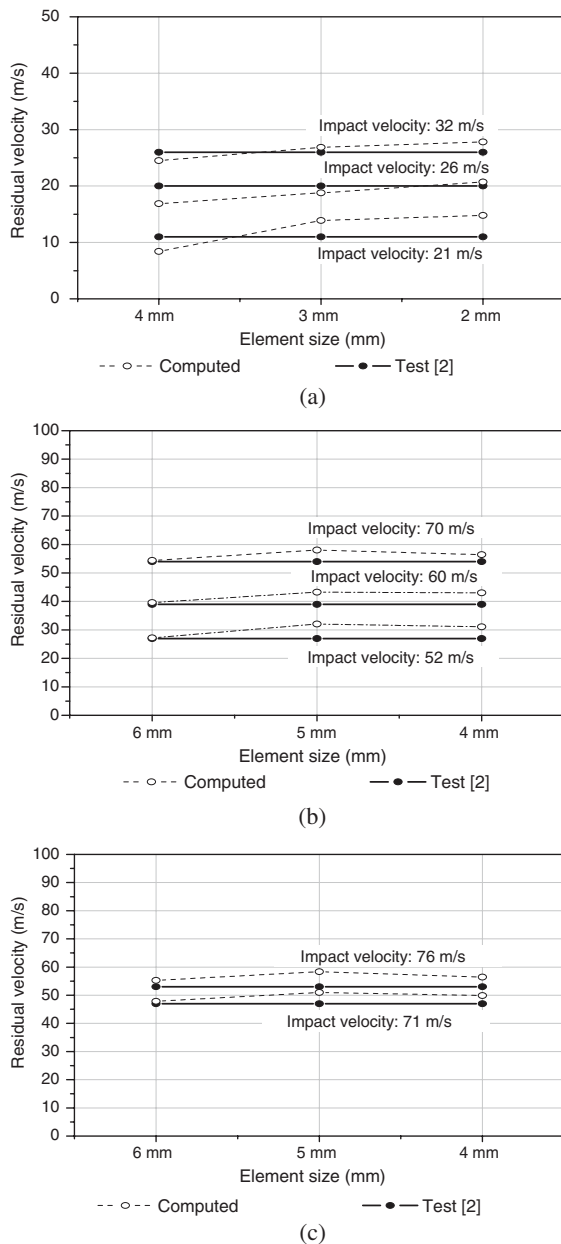$$CI = 1 - \frac{\sqrt{(\sum e_i^2)}}{\sum V_r} \qquad (2)$$

Fig. 7 Mesh convergence study for (a) 0.5 mm; (b) 1.5 mm; and (c) 2.0 mm thick aluminium target plates
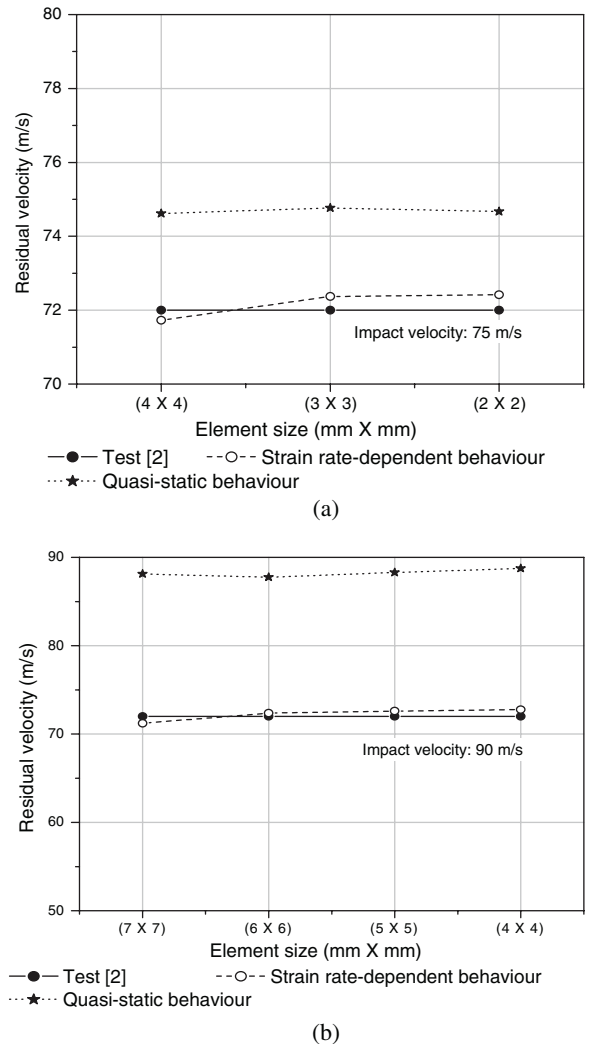

Fig. 8 Effect of ignoring material strain rate sensitivity on computed residual velocity for (a) 0.5 mm and (b) 2 mm thick plates

where V_r is the test residual velocity, e_i is the difference between computed and test residual velocities, and the summation is carried out over the number of cases for which a combined index of correlation is sought. It is apparent from equation (2) that as the degree of correlation increases, CI approaches unity. A CI value of 0.92 has been obtained from Fig. 7 by considering all converged residual velocities. It may be concluded from Fig. 7 that shell elements of size 2–4 mm may be used for analysing thin aluminium targets with CESS interface in LS-DYNA.

4 EFFECT OF STRAIN RATE-DEPENDENT MATERIAL MODELLING OF TARGET ON PROJECTILE RESIDUAL VELOCITY

One of the key aspects of finite-element modelling is the adoption of strain-rate-dependent material behaviour as discussed previously in section 2.1. The effect of strain rates is assessed by repeating the residual velocity convergence study carried out in the previous section for plates of 0.5 and 2 mm thickness by assigning quasi-static properties only to the plate material, and ignoring strain-rate-sensitive yield and ultimate strengths. It is seen in Fig. 8 that ignoring material strain rate sensitivity has a noticeable effect on computed residual velocities that turn out to be significantly higher than the corresponding test-based values. This is a consistent outcome as usage of quasi-static properties at high strain rates is tantamount to using a weaker plate.

5 BALLISTIC LIMIT PREDICTION AND OTHER PARAMETRIC STUDIES

With the help of the mesh configuration and material modelling procedure that yielded desirable residual velocities in convergence studies reported already, a number of parametric studies are next carried out

by varying target plate thickness as well as projectile geometry and mass. The ballistic limits obtained through simulation are compared with corresponding experimental data to establish the power of present modelling approach as an efficient and reliable technique for designing penetration-resistant armours.

5.1 Definition of ballistic limit

Ballistic limit is an essential index for evaluating projectile and armour performance and is defined in reference [5] as 'the average of two striking velocities, one of which is the highest velocity giving a partial penetration and the other which is the lowest velocity giving a complete penetration'. In the present study, ballistic limit is interpreted as the minimum impact velocity at which zero residual velocity is first encountered. Thus, referring to Fig. 9 which depicts velocity time histories of projectiles normally impacting a 1.5 mm thick target plate, 43.5 m/s can be considered as the ballistic limit as a slightly higher impact velocity results in a non-zero residual velocity.

5.2 Effect of plate thickness on ballistic limit and perforation energy

Computed ballistic limits and perforation energies are plotted in Fig. 10 with respect to plate thickness. Both the ballistic limit and perforation energy display rising trends with increasing plate thickness as observed in tests reported in reference [2]. A CI value of 0.92 is obtained from Fig. 10 for all data points considered, which shows that a great degree of correlation exists between experimental data and the computed results obtained here.

5.3 Effect of projectile mass on ballistic limit and perforation energy

The effect of changing projectile shank length leads to a change in projectile aspect ratio (l/d) and its mass.
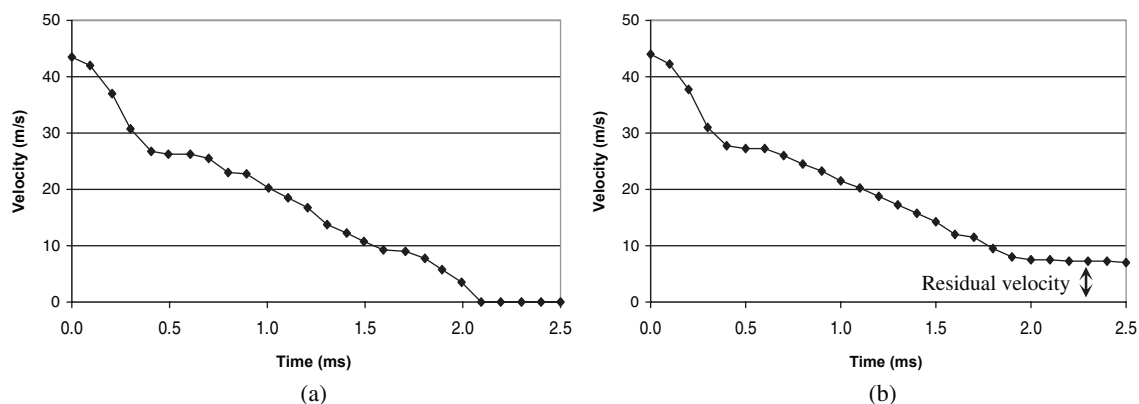

(a)

(b)

Fig. 9 Computed velocity time histories for 1.5 mm thick target plates with normal impact speeds of (a) 43.5 m/s and (b) 44 m/s
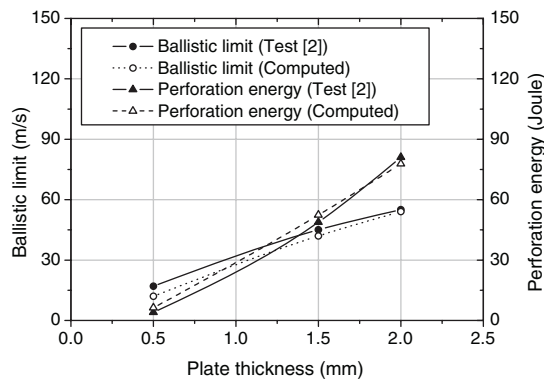
Fig. 10 Variations of ballistic limit and perforation energy with respect to plate thickness
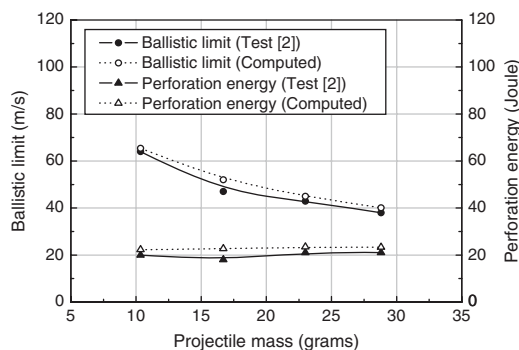

Fig. 11 Variations of ballistic limit and perforation energy with respect to projectile mass

It has been found in reference [2] and shown in Fig. 11 that increasing projectile mass in this manner actually decreases its ballistic limit; however, perforation energy is found to be relatively insensitive to change in projectile mass when diameter is kept as constant. A comparison is made between the computed ballistic limits and perforation energies for varying projectile mass with the corresponding test-based values in Fig. 11 and extremely good correlation confirmed by a CI value of 0.94 is observed.

5.4 Effect of projectile nose shape on residual velocity

The investigators in reference [4] studied the relative performance of blunt- and hemispherical-nosed projectiles during impact on thin aluminium plates. The numerical simulations were carried out in reference [4] using two-dimensional elements exploiting axisymmetry and employing the ABAQUS code. Following the present finite-element procedure and carrying out analysis with LS-DYNA, a comparison is made in Fig. 12 between the computed results and the corresponding test data given in reference [4]. A CI value of 0.97 obtained for all cases in Fig. 12 indicates a high degree of correlation with test data.
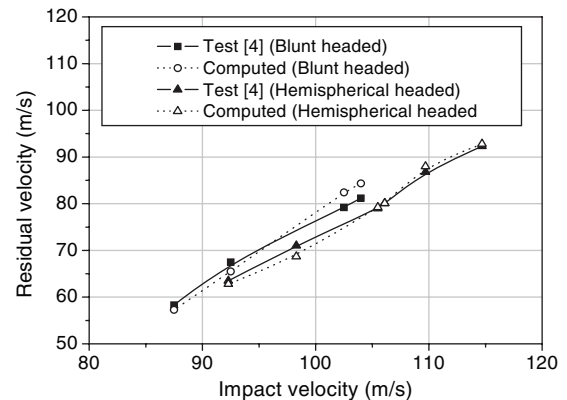

Fig. 12 Comparison of residual velocities for impact with blunt and hemispherical projectiles of 19 mm diameter

5.5 Simulation-based failure modes

In laboratory tests of impact on thin aluminium plates, an impinging projectile causes yielding and crack formation in plate material directly on its path leading to perforation, and dishing in the rest of the plate [2]. Views of a typical thin aluminium plate before and after perforation by an ogival-nosed projectile are shown in Figs 13(a) and (b), respectively. An analysed plate in Fig. 13(c) shows the formation of dishing, and jaggedness along the edge of perforation similar to the 'petalling' phenomenon seen in tests. A planar view of the analysed plate in Fig. 13(d) shows the formation of a circular hole in the plate similar to what was obtained in tests.

It is again pointed out that the impact testing on armour plates are costly and time-consuming. Hence, the available test results from references [2] and [4] have been used for the validation of numerical results obtained through the current analysis and are shown in Figs 7 to 13.

6 IN-HOUSE EXPERIMENTS

Previous sections of this article have dealt with the development of a powerful finite-element modelling approach for prediction of residual velocity and ballistic limits for impact on thin aluminium plates. Various aspects of finite-element modelling that can have significant effect on computed results have been considered. These include representation of the physical plate with shell elements, size of elements, constitutive modelling with strain rate effects, contact type, etc. Despite the robust correlation achieved against published experimental results, it would be prudent to conduct one's own experiments, for a final correlation via the present modelling procedure and analysis with the explicit LS-DYNA 970 solver. With this aim in mind, tests have been carried out on commercial grade
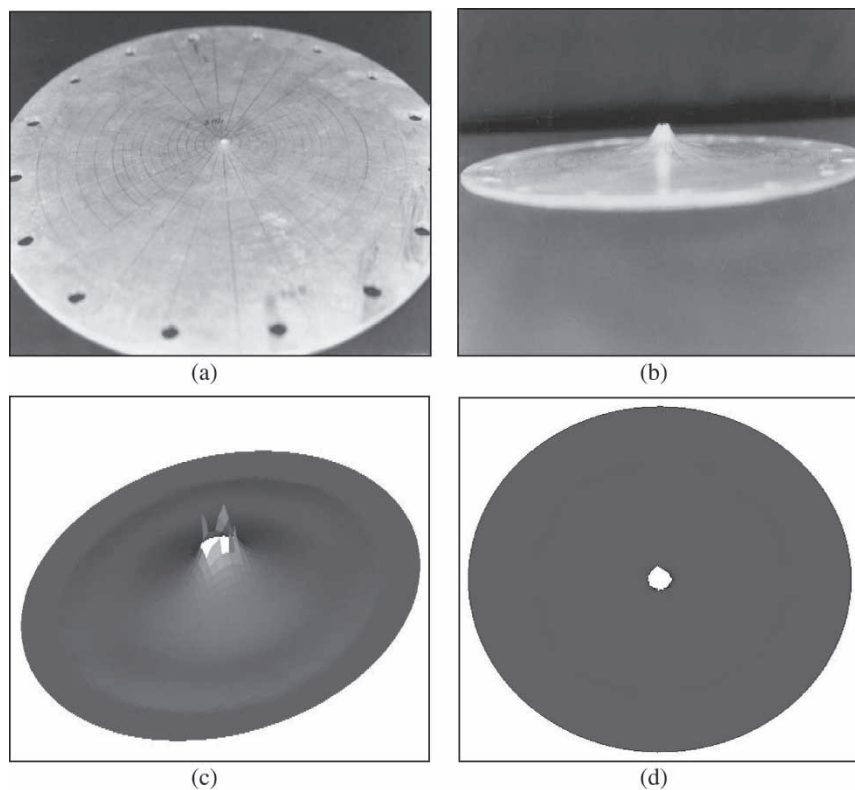
Fig. 13   (a) Plate before impact test [2]; (b) perforated plate after impact test [2]; (c) perforated plate after analysis showing petalling and dishing; and (d) planar view of plate after analysis indicating a nearly circular hole
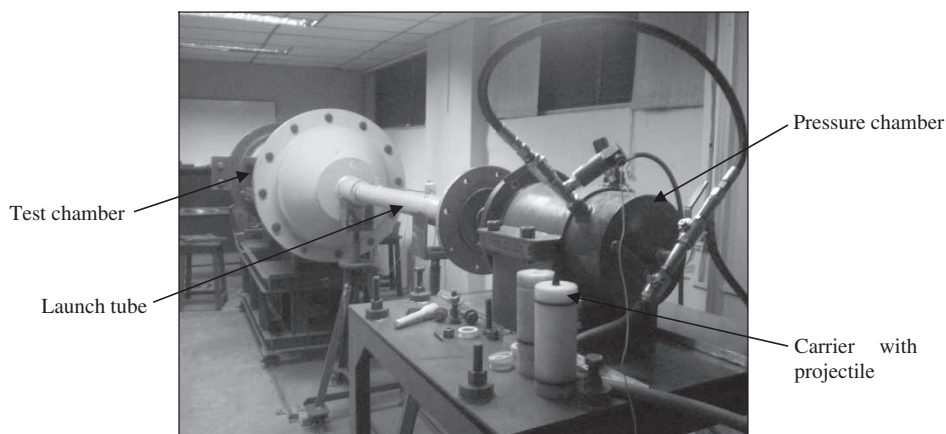

Fig. 14   Ballistic impact testing facility in Product Safety Laboratory, CPDM, IISc

1100 aluminium plates of 1 mm thickness with projectiles of four different nose shapes. A sophisticated ballistic impact testing facility as shown in Fig. 14 and a high-speed camera have been used for the present experiments.

Commercially available grade 1100 aluminium plates of 1 mm thickness has been cut into pieces of the required dimensions and shape (circular shape with a diameter of 255 mm) followed by trimming of edges. Projectiles of different nose shapes such as conical,

ogival, hemispherical, and blunt all with a diameter of 15 mm are turned from mild steel rods and subsequently hardened to a hardness range of 50–52 R_c. The mass of the projectile is kept constant by altering its length for each nose shape. Each finished projectile weighed 55 ± 0.1 g. Target plates were rigidly held in a fixture with a free span of 205 mm diameter. The projectile is placed in a carrier and the whole set has been then inserted into the pressure chamber. The pressure chamber and launch tube were connected rigidly with

a number of bolts and the vacuum pump turned on. The pressure chamber is filled to the required pressure by opening a valve connected to a nitrogen gas cylinder; finally the vacuum pump is switched off and the projectile launched. A high-speed camera is activated just prior to the projectile launch and the impact event recorded.

The computed resultant impact and residual velocities of all the projectiles are listed in Table 3. In the present case, the velocity is measured by considering the displacement of the projectile nose divided by the time taken between two successive frames of the high-speed camera record. The recorded images at various instants of time for the grade 1100 aluminium plates impacted by conical-, ogival-, hemispherical-, and blunt-nosed projectiles are shown in Fig. 15.

As seen in Fig. 15, complete penetration occurred at the time frame of $2500\,\mu s$ for all the four test cases; however, the initial penetration differed according to the nose shape of the projectile. The failure

Table 3 Computed resultant velocities of projectiles for the different test cases

Projectile nose shape	Plate thickness (mm)	Impact velocity (m/s)	Angle of obliquity (degrees)	Recorded resultant residual velocity (m/s)
Conical	1.0	32.04	5.70	25.70
Ogival	1.0	30.70	15.89	24.10
Hemispherical	1.0	33.87	14.49	25.73
Blunt	1.0	34.79	4.80	23.10

pattern also varied with the projectile nose shape as shown in Fig. 16. It may be noted from Fig. 16 that the perforation caused by conical-, ogival-, and hemispherical-nosed projectiles is associated with petalling behaviour; however, in the case of blunt projectile impact, no clear plug formation is seen and a nearly circular plug is formed, which remained thinly attached to the hole boundary.
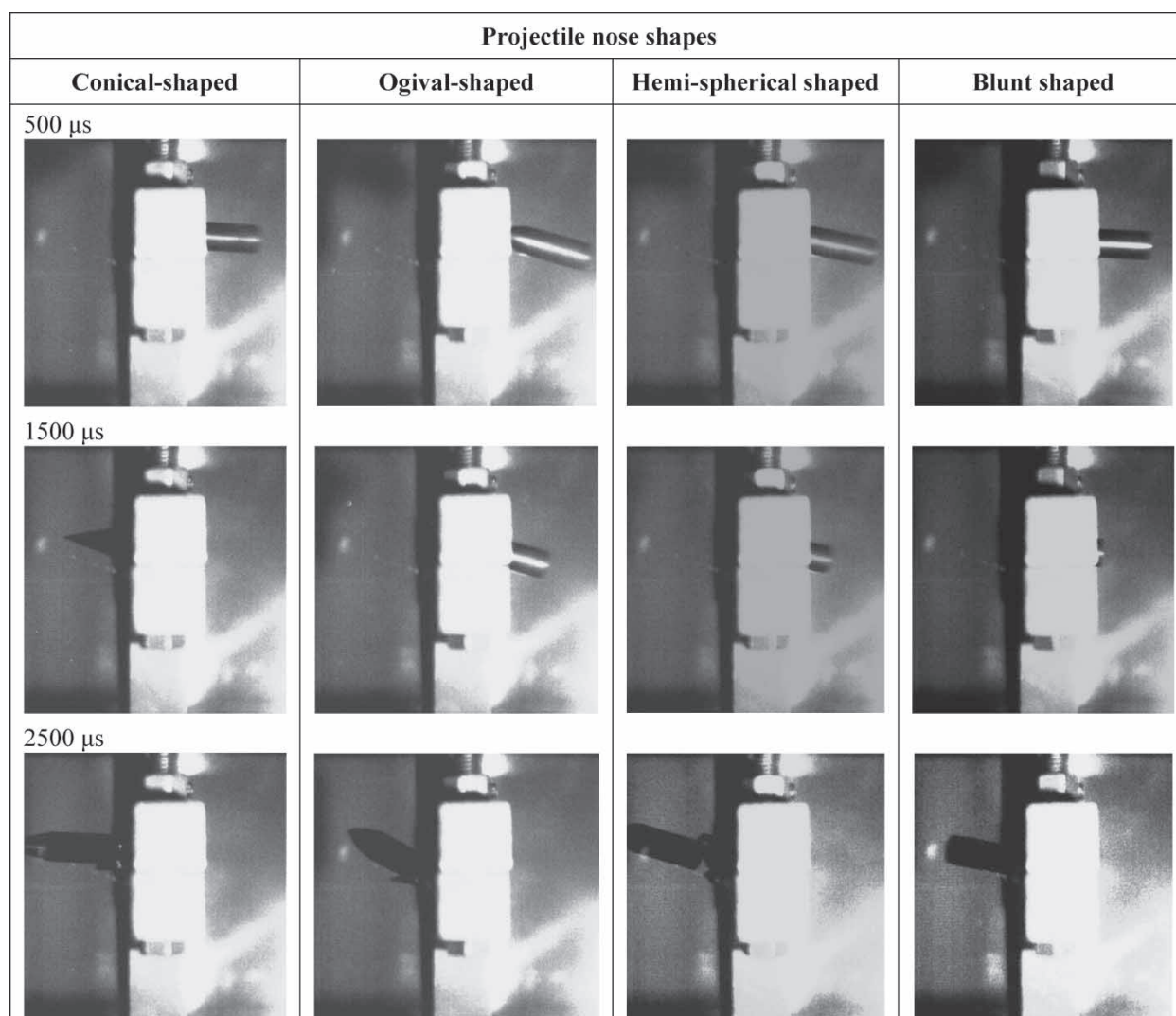

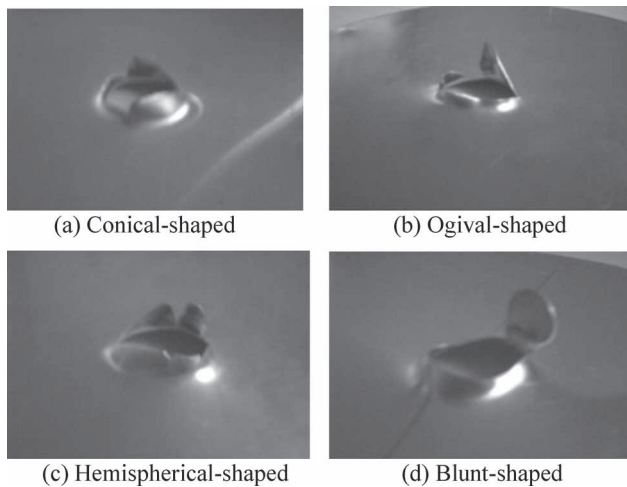**Fig. 15** Recorded images at various instants of time

(a) Conical-shaped

(b) Ogival-shaped

(c) Hemispherical-shaped

(d) Blunt-shaped

Fig. 16 Truncated views of the target plate after the completion of penetration

7 FURTHER VALIDATION OF THE NUMERICAL PROCEDURE

The finite-element modelling procedure described in section 3 has been used for simulating the current test cases. The finite-element models of target plate and projectile using BLT shell elements of 2 mm size and solid elements, respectively, are shown in Fig. 17. The

shape and size of the target plate and projectile and the impact conditions considered for modelling were the same as the test cases defined in Table 3.

Simulations were carried out for the four test cases corresponding to the four different shaped projectiles. The impact velocities measured in the four tests considered are given in Table 3 and each of these is the specified projectile initial velocity in the simulation. The angle of obliquity of impact is also specified by rotating the projectile from its normal axis according to the measured values of the angles given in column 4 of Table 3. The resultant residual velocity predicted in each case through analysis is compared with the test-based residual velocity in Table 4 and an excellent correlation is seen with a maximum deviation between computed and observed residual velocities of only 4.3 per cent. It may be noted that the use of the high-speed camera made possible a very accurate assessment of the initial angle of obliquity as well as the resultant residual velocity in the direction of motion of the projectile after plate perforation.

Truncated close-up views of actual and simulated plate failures are compared in Table 5. In the first three cases of perforation by conical-, ogival-, and hemispherical-nosed projectiles, plate failure in the tests is associated with petalling but no clear plug formation; similar failure patterns are also obtained through analysis. For the last case of blunt projectile
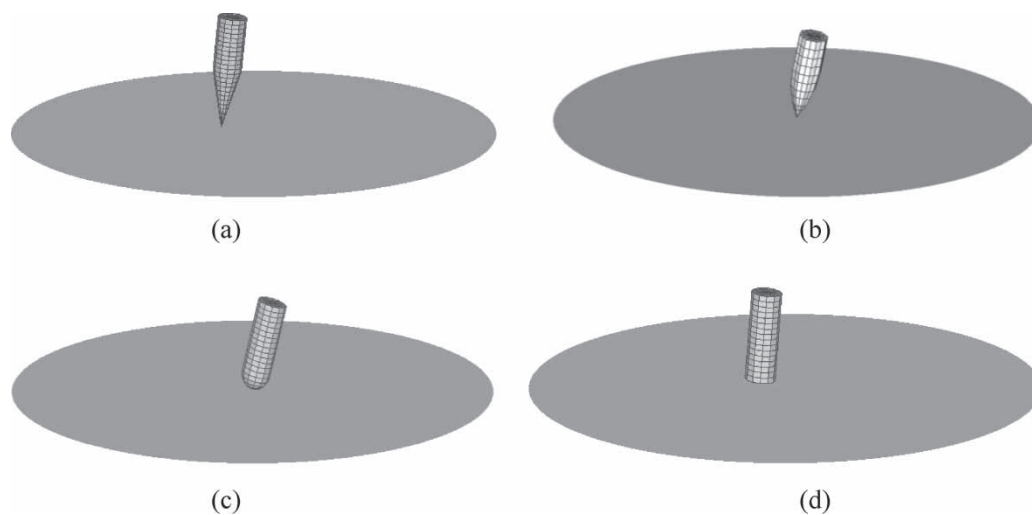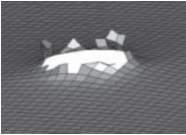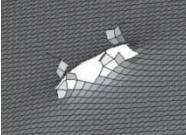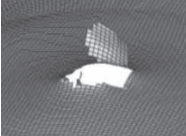

Fig. 17 Finite-element models of circular target plates with slightly oblique: (a) conical-head; (b) ogival-head; (c) hemispherical-head; and (d) blunt-head projectiles (before impact)
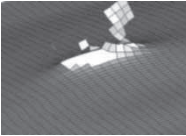
Table 4 Comparison of projectile residual velocity for different nose shapes

Projectile nose shape	Plate thickness (mm)	Impact velocity (m/s)	Angle of obliquity (degrees)	Resultant residual velocity (m/s)		% Deviation from test
				Test	Simulation	
Conical	1.0	32.0	5.7	25.7	25.1	−2.3
Ogival	1.0	30.7	15.9	24.1	23.8	−1.2
Hemispherical	1.0	33.9	14.5	25.7	24.9	−3.1
Blunt	1.0	34.8	4.8	23.1	22.1	−4.3

Table 5 Close-up views of actual and simulated plate failures

Projectile nose shape	Experiment	Simulation
Conical-head		
Ogival-head		
Hemispherical-head		
Blunt-head		

impact, a nearly circular plug is formed which remained thinly attached to the hole boundary; a strikingly similar plug is seen in the simulation perforation. The extremely good correlation of simulation results of projectile residual velocity and plate failure modes with corresponding test data presented in this section confirm that the present finite-element modelling procedure using LS-DYNA is an excellent tool for the assessment and design of thin aluminium armour plates subject to near-normal impacts.

8 CONCLUDING REMARKS

This article details a comprehensive numerical study and accurate prediction of ballistic limits of projectiles for normal impact on thin aluminium plates. The material modelling included a relatively straightforward inclusion of strain effects on yield and failure strengths as well as uniaxial failure strain. The elasto-plastic deformations and failure are governed by shear energy criteria for ductile materials as embodied in von Mises yield criterion together with an associative flow rule of plasticity and isotropic strain hardening. Effects of mesh density and non-inclusion of strain rate effects in constitutive modelling have been studied. It has been shown in a number of cases by comparing with test data that the present modelling and analysis procedure using LS-DYNA is consistently able to predict the effects of plate thickness, projectile mass, and projectile nose shape on ballistic limit and residual velocity. The failure modes obtained through simulation are also realistic when compared to observed plate deformation and perforation in experiments. Experiments have been conducted on 1 mm thick aluminium plates for four different noses and numerical simulations have also been carried out in order to validate the simulation guidelines developed in the present study. Finally, it is concluded that the finite-element modelling procedure using LS-DYNA is an excellent tool for designing thin aluminium armour plates for protection against low-calibre projectiles.

© Authors 2009

REFERENCES

1 **Gupta, N. K.** and **Madhu, V.** An experimental study of normal and oblique impact of hard-core projectile on single and layered plates. *Int. J. Impact Eng.*, 1997, **19**, 395–414.
2 **Gupta, N. K., Ansari, R.,** and **Gupta, S. K.** Normal impact of ogival nosed projectiles on thin plates. *Int. J. Impact Eng.*, 2001, **25**, 641–660.
3 **Khan, W. U., Ansari, R.,** and **Gupta, N. K.** Oblique impact of projectile on thin aluminium plates. *J. Def. Sci.*, 2003, **58**(2), 139–146.
4 **Gupta, N. K., Iqbal, M. A.,** and **Sekhon, G. S.** Experimental and numerical studies on the behaviour of thin aluminium plates subjected to impact by blunt- and hemispherical-nosed projectiles. *Int. J. Impact Eng.*, 2006, **32**(12), 1921–1944.
5 **Corran, R. S. J., Shadbolt, P. J.,** and **Ruiz, C.** Impact loading of plates – an experimental investigation. *Int. J. Impact Eng.*, 1983, **1**(1), 3–22.
6 **Backman, M. E.** and **Goldsmith, W.** The mechanics of penetration of projectile into targets. *Int. J. Eng. Sci.*, 1978, **16**, 1–99.
7 **Borvik, T., Langseth, M., Hopperstad, O. S.,** and **Malo, K. A.** Perforation of 12 mm thick steel plates by 20 mm diameter projectiles with flat, hemispherical and conical noses: part I: experimental study. *Int. J. Impact Eng.*, 2002, **27**, 19–35.
8 **Kad, B. K., Schoenfeld, S. E.,** and **Burkins, M. S.** Through thickness dynamic impact response in textured Ti-6Al-4V plates. *Mater. Sci. Eng. A*, 2002, **322**, 241–251.
9 **Lim, C. T., Shim, V. P. W.,** and **Ng, Y. H.** Finite-element modelling of the ballistic impact of fabric armour. *Int. J. Impact Eng.*, 2003, **28**, 13–31.
10 **Tan, V. B. C., Lim, C. T.,** and **Cheong, C. H.** Perforation of high strength fabric by projectiles of different geometry. *Int. J. Impact Eng.*, 2003, **28**, 207–222.
11 **Nandlall, D., Williams, K.,** and **Vaziri, R.** Numerical simulation of the ballistic response of GRP plates. *Comput. Sci. Technol.*, 1998, **58**, 1463–1469.
12 **Park, M., Yoo, J.,** and **Chung, D.-T.** An optimisation of multi-layered plate under ballistic impact. *Int. J. Solids Struct.*, 2005, **42**, 123–137.

13 **Fawaz, Z., Zheng, W.,** and **Behdinan. K.** Numerical simulation of normal and oblique ballistic impact on ceramic composite armours. *Compos. Struct.*, 2004, **63**, 387–395.

14 **Borvik, T., Langseth, M., Hopperstad, O. S.,** and **Malo, K. A.** Perforation of 12 mm thick steel plates by 20 mm diameter projectiles with flat, hemispherical and conical noses: part II: numerical study. *Int. J. Impact Eng.*, 2002, **27**, 37–64.

15 **Martineau, R. L., Prime, M. B.,** and **Duffey, T.** Penetration of HSLA-100 steel with tungsten carbide spheres at striking velocities between 0.8 and 2.5 km/s. *Int. J. Impact Eng.*, 2004, **30**, 505–520.

16 **Prakash, T., Sekhon, G. S.,** and **Gupta, N. K.** Adaptive finite element analysis of plastic deformation of plates under projectile impact. *J. Def. Sci.*, 2003, **53**(1), 57–65.

17 **Raguraman, M., Deb, A.,** and **Gupta, N. K.** A numerical study of projectile impact on mild steel plates. *Curr. Sci.*, 2007, **93**, 498–506.

18 **Deb, A., Raguraman, M., Gupta, N. K.,** and **Madhu, V.** Numerical simulation of projectile impact on mild steel armour plates using LS-DYNA, part I: validation. *Def. Sci. J.*, 2008, **58**, 422–438.

19 Available from www.matweb.com.

20 **Borvik, T., Hopperstad, O. S., Berstad, T.,** and **Langseth, M.** A computational model of viscoplasticity and ductile damage for impact and penetration. *Eur. J. Mech. A/Solids*, 2001, **20**, 685–712.

21 **Weoi-Shyan, L., Jia-Chyuan, S.,** and **Su-Tang, C.** Effect of strain rate on impact response and dislocation substructure of 6061 T6 aluminium alloy. *Scr. Mater.*, 2000, **42**, 51–56.